Comparison of Thermal Numerical Simulation Data with Experimental Data from the ISCT 200-US Permanent Magnet Hall Thruster

Marconi C. Porto, Alexandre A. Martins, José Leonardo Ferreira & Carlos Humberto Llanos

University of Brasilia

ABSTRACT

Due to its great efficiency, the Plasma Physics Laboratory of the Physics Institute of the University of Brasilia (PPL/PI/UnB) has been developing Hall thrusters since 2004. Testing NeFe and SmCo permanent magnets, excellent results were achieved with the PHALL II series (PPL). However, permanent magnets have limitations due to the working temperature (determined by the Curie temperature). Therefore, it is necessary to strictly control its temperature to avoid the demagnetization effect.

In this work, the results of the numerical thermal simulation were compared with experimental temperature results for the ISCT200-US Hall Thruster in order to verify the reliability of the simulation tool, allowing its future use in simulations of other Hall thrusters. Experimental temperature values and, whenever possible, dimensions and materials of the propellant components were collected from references on the ISCT200-US. A mechanical drawing of the ISCT 200-US was created, a numerical thermal simulation was developed, temperature simulation values were collected and compared with experimental values.

Keywords: hall thruster electric propulsion thermal numerical simulation ISCT 200-US thermal dissipation aerospace.

Classification: LCC Code: TL787-TL4050

Language: English

Great Britain Journals Press

LJP Copyright ID: 392922
Print ISSN: 2631-8474
Online ISSN: 2631-8482

London Journal of Engineering Research

Volume 23 | Issue 5 | Compilation 1.0

Comparison of Thermal Numerical Simulation Data with Experimental Data from the ISCT 200-US Permanent Magnet Hall Thruster

Marconi C. Porto[α], Alexandre A. Martins[σ], José Leonardo Ferreira[ρ] & Carlos Humberto Llanos[ω]

ABSTRACT

Due to its great efficiency, the Plasma Physics Laboratory of the Physics Institute of the University of Brasilia (PPL/PI/UnB) has been developing Hall thrusters since 2004. Testing NeFe and SmCo permanent magnets, excellent results were achieved with the PHALL II series (PPL). However, permanent magnets have limitations due to the working temperature (determined by the Curie temperature). Therefore, it is necessary to strictly control its temperature to avoid the demagnetization effect.

In this work, the results of the numerical thermal simulation were compared with experimental temperature results for the ISCT200-US Hall Thruster in order to verify the reliability of the simulation tool, allowing its future use in simulations of other Hall thrusters. Experimental temperature values and, whenever possible, dimensions and materials of the propellant components were collected from references on the ISCT200-US. A mechanical drawing of the ISCT 200-US was created, a numerical thermal simulation was developed, temperature simulation values were collected and compared with experimental values. A coherent comparison was achieved, which demonstrated the reliability of the simulation tool. Such results are important for the space qualification of thrusters subsequent to the PHALL II series.

Keywords: hall thruster electric propulsion thermal numerical simulation ISCT 200-US thermal dissipation aerospace.

Author α σ ρ: Plasma Physics Laboratory, Physics Institute, University of Brasilia, Brasilia, Brazil.

α ω: Embedded Systems and Integrated Circuit Applications Laboratory, Mechanical Engineering Department, University of Brasilia, Brasilia, Brazil.

I. INTRODUCTION

Hall thrusters are considered a type of electric thruster [1-6]. The main characteristic of an electric thruster is the ability to produce plasma by ionization of a neutral gas, by the inclusion of electric and magnetic fields in its medium, and generate impulse for its acceleration of the thruster. Normally used to correct the orbit and attitude of artificial satellites and the propulsion of space probes, the Hall thruster has as its basic shape a cylindrical channel, an anode at the bottom of this channel, a magnetic field inside the channel and an external cathode [6]. Its operation consists of injecting a neutral gas into the channel, emitting electrons from the cathode towards the anode; the thruster then confines the electrons in an ExB Hall current that creates a virtual cathode above the anode. In this way, the electric field between the anode and the virtual cathode accelerates the ions out of the channel, generating thrust. The first flight tests of the Hall thruster took place in the 1960s [1,5–7].

The Physics Laboratory of the Physics Institute of the University of Brasília (PPL/PI/UnB) has been developing Hall Thrusters since 2004 [1,2,8,9] under the name PHALL Project. It is an incremental project, having started with PHALL I, followed by PHALL II-A, PHALL II-B and currently the PHALL II-C version (Fig. 1 and 2). The current version has a TRL 3 classification (Technology Readiness Level, NASA). The next, more compact and efficient version, to be developed by PPL, supported by the Brazilian

Space Agency (AEB), is the PHALL III [1] to reach TRL 6. The ultimate objective is to develop a Hall thruster for micro and small aritifical satellites fully qualified for spaceflight with TRL 9 classification. Other PPL work includes an HPT thruster (Fig. 3) in different versions, elimination of biological contaminants using plasmas and deposition of thin carbon films.

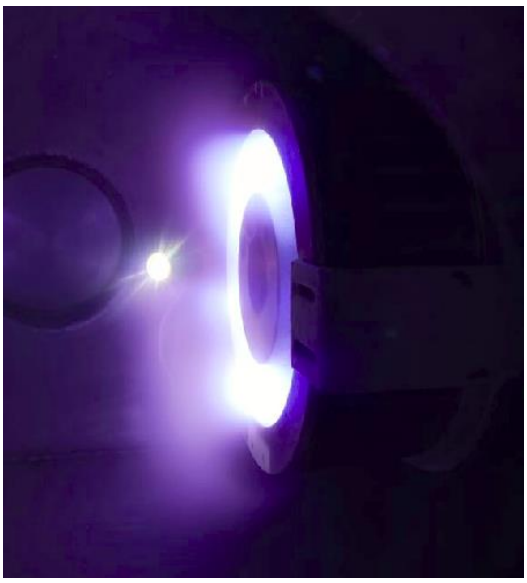

Fig. 1: Side View of PHALL II-C in Operation (PPL/PI/UnB)

The present work aims to verify the reliability of a thermal numerical simulation strategy and corroborate the results obtained in a similar work carried out by PPL with the BPT-4000 thruster [11]. Such confirmation will allow future tests with PHALL III and its subsequent versions.

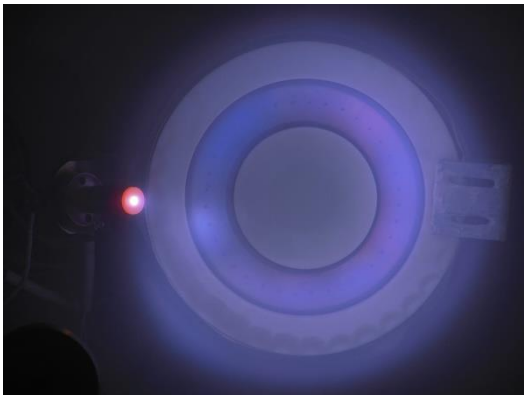

Fig. 2: Front view of PHALL II-C in operation (PPL/PI/UnB)

A systematic bibliographic research was carried out to find articles in which Hall thruster experiments with sufficient data to perform a simulation were presented. No studies were found that compared results from experiments and thermal simulations. Thus, the main advantage of the results of this study in relation to other experimental and thermal simulation studies is the fact that they indicate good reliability for commercial simulation software widely used in relation to thermal simulations of Hall Thrusters. In this research, few options were found, two of which were advantageous for developing work like this: one option was the Hall BPT4000 thruster (discharge power of 4500 W, electromagnetic coils), the study of which was developed by PPL in [11]; and the other option was the Hall ISCT200-US thruster (200 W discharge power, permanent magnets), the study of which is developed in the present work. The study carried out proposes to carry out a study that presents a good approximation between the

contexts of the PHALL II-C and ISCT200-US thrusters and not necessarily something extremely precise or exact to give direction to future work that approach thermal numerical simulations through the technique of finite elements.

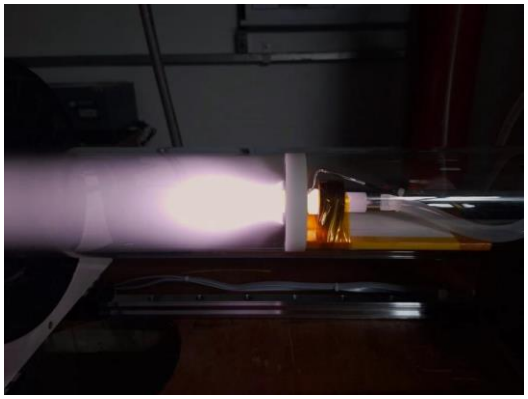

Fig. 3: HPT Thurster in Operation (PPL/PI/UnB)

The experimental data of the ISCT 200-US thruster [10] was collected from the literature and then thermal numerical simulation of this thruster was carried out. The simulation temperatures obtained were compared with the experimental ones, observing a good agreement with experimental data, with a small percentage difference. This fact indicates that this approach, based on finite elements, has good reliability on the Hall thruster simulation task, in addition to corroborating the results found in [11] for the BPT-4000 thruster.

Two software were considered to be used in the simulations, SolidWorks 2017 and Ansys 2017. Although a detailed benchmark was not performed, the Solid Works 2017 software proved to be the best option because the thermal model used by this software was found, but was not found for Ansys 2017 software. Additionally, SolidWorks 2017 has simpler CAD handling and is probably better known.

In future PPL work, supported by AEB, we will carry out an experiment to thermal study the PHALL III (next version) and, later, we will carry out a more precise comparison study with simulation software.

The main contributions of the present work are the following: (a) a verification of the reliability of a thermal numerical simulation of Hall thrusters (such a comparison between simulation and experiment was not found in the literature), (b) a verification of the equations for dissipated thermal powers in Hall thrusters (definition of an appropriate configuration of equations to support the system modeling problem using the finite element technique), (c) Corroboration of the results of this work with the results obtained in [11], with the exception that, this time, the thruster's magnetic field is generated by permanent magnets.

As a description of the sections of the article, we have: (a) section 2, which describes the methodology, (b) section 3, which presents the mathematical models, (c) section 4, with the results and their analysis, and (d) section 5, presenting the most relevant conclusions.

II. METHODOLOGY

Below is, in summary form (with greater detail in the subsections), the procedure adopted.

1) From reference [10], the experimental temperatures of the ISCT 200-US thruster were collected.
2) The thermal power dissipated generated by the thruster was calculated.
3) The materials for the ISCT 200-US components were selected.
4) The 3D CAD mechanical drawing was copied from the references.
5) Simulated and experimental temperature data were compared.

2.1 Experimental Temperatures

From Ref. [10], the average experimental temperatures were consulted in the following parts of the thruster: anode, internal wall and external wall (blue in Fig. 4).

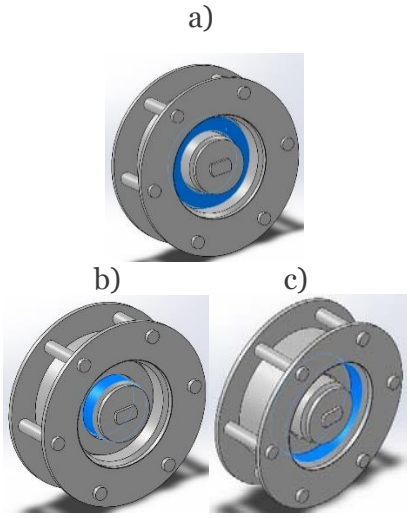

Fig. 4: Regions (in blue) of the ISCT200-US Where Experimental Temperatures Were Measured: (A) Anode, (b) Inner Wall, and (c) Outer Wall

Such temperatures are given in Table 1. No data were found in the literature on thermal contact resistances related to ISCT 200-US. Another way to obtain this data would be throu h tem erature measurement in experiments on a real physical model, which was not viable. Therefore, thermal contact resistances were disregarded in the simulation.

Table 1: Average Experimental Temperatures of the ISCT 200US

ISCT200-US	Anode (°C)	Inner Wall (°C)	Outer Wall (°C)
Experiment	440.00	420.00	413.00

2.2 Dissipated Termal Powers

The following steps were followed in order to determine the dissipated thermal powers used in the ISCT 200-US simulation: some internal experimental data from PHALL II-C (such as, for example, plasma potential, floating potential and electron density) were used in the model for thermal energy dissipation [6,12] to calculate the power dissipated in PHALL II-C. After that, using the power dissipated in the PHALL IIC, the power dissipated in the ISCT 200-US was calculated proportionally to the discharge power of the PHALL II-C (subsection 3.1).

2.3 ISCT 200-US materials and mechanical drawing

With the help of information found in works [10,14,15,17], the mechanical drawing in 3D CAD was generated. Fig. 5 shows the exploded view of the mechanical drawing. Because they have little influence on heating and to speed up the simulation process, the fasteners were omitted. Fig. 6 shows a perspective view of the assembled thruster. In Table 2, you can find the main measurements of the mechanical drawing of the ISCT200-US compared to the measurements of the PHALL II-C. And in Fig. 7, there is a perspective view of PHALL II-C.

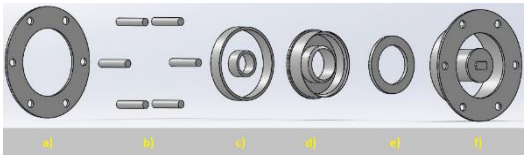

Fig. 5: Exploded View of the Mechanical Drawing of the ISCT200-US Thruster. From Left to Right: (a) Base Piece, (b) 6 Tubes for Heat Transmission, (c) Representation of Permanent Magnets, (d) Ceramics, (e) Anode, and (f) Structure

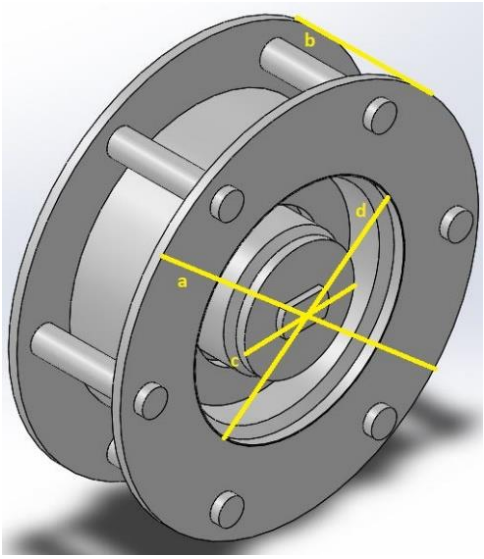

Fig. 6: Perspective View of the Mechanical Drawing of the ISCT200-US Thruster

The materials were consulted in works [10,14-17] related to the ISCT 200-US thruster, as far as possible. When there was not enough information, the same materials (or similar materials) as the PHALL II-C thruster were used. The materials used in the simulation are presented with the relevant physical properties in Table 3.

Table 2: Main measurements of the Mechanical Drawing for the Simulation of the ISCT200-US (Figure 6) and the PHALL II-C (Figure 7)

Part of the Thruster	Values (mm)	
	ISCT200-US	PHALL II-C
Front View Diameter	85.00 (a)	151.40 (e)
Length	26.50 (b)	82.28 (f)
Discharge Channel Internal Diameter	26.00 (c)	68.01 (g)
Discharge Channel External Diameter	49.50 (d)	114.14 (h)

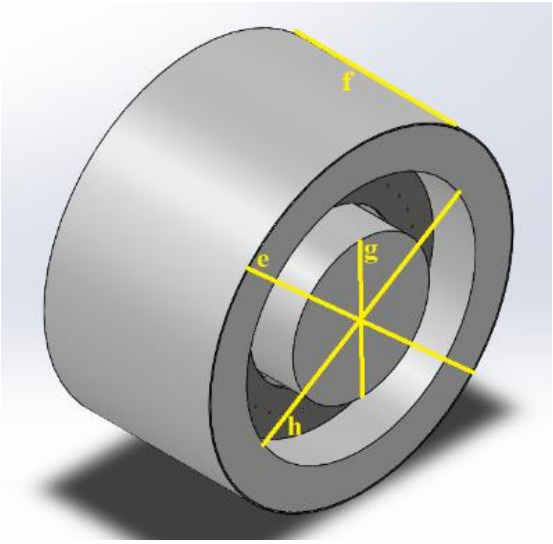

Fig. 7: Perspective View of the Mechanical Drawing of the PHALL II-C Thruster

Table 3: Materials of the ISCT200-US Components and Their Physical Properties

Component	Material	Mass Density (kg/m^3)	Thermal Conductivity (W/mK)	Specific Heat (J/kgK)	Emissivity
Structure	Stainless Steel 301	7880.00	21.40	500.00	0.59
Base Piece	Stainless Steel 301	7880.00	21.40	500.00	0.59
Anode	Stainless Steel 304 [16,17]	8000.00	16.20	500.00	0.19
Ceramics	BN-SiO_2 [10,14-17]	2100.00	11.00	770.00	0.90
Tubes	Copper [16,17]	8900.00	390.00	390.00	0.75
Permanent magnets	Sm_2Co_{17} [16,17]	8400.00	11.63	376.81	0.11

III. MATHEMATICAL MODELS

3.1 Model for Thermal Energy Dissipation

The dissipated thermal power values used for the ISCT200-US thruster simulation were calculated proportionally to the same values for the PHALL II-C thruster. To calculate the dissipated thermal powers of the PHALL II-C, a model for thermal energy dissipation in Hall thrusters [6,12] was used, into which the thruster thruster plasma data can be inserted. The equation for the discharge power P_d [12] is:

$$P_d = P_b + P_w + P_a + P_r + P_{ions}, \quad (1)$$

where P_b is the beam power, P_w is the power dissipated in the walls, P_a is the power dissipated in the anode, P_r is the radiative power loss from the plasma, and P_{ions} is the power to produce ions.

The beam power is defined by the equation:

$$P_b = V_b I_b, \quad (2)$$

where V_b is the beam voltage, I_b is the beam current. The following equation is the power dissipated in the walls:

$$P_w = n_e e A_w \left[\left(\frac{kT_e}{e}\right)^{\frac{3}{2}} \left(\frac{2e}{\pi m}\right)^{\frac{1}{2}} e^{\frac{e\phi_S}{kT_e}} + \frac{1}{2}\left(\frac{kT_e}{M}\right)^{\frac{1}{2}} (\varepsilon - \phi_S) \right], \quad (3)$$

where n_e is the electronic density, e is the electron charge with positive value, A_w is the surface area of the wall in contact with the plasma, k is the Boltzmann constant, T_e is the temperature electronic in Kelvins, m is the electron mass, ϕ_S is the sheath potential relative to the plasma ($-V_f$), M is the mas of the Argon atom (PHALL II-C propellant), and ε is the pre-sheath ion energy. The power dissipated in the anode can be calculated by the following equation:

$$P_a = 2T_{eV}I_a \approx 2T_{eV}I_d, \quad (4)$$

where T_{eV} is the electronic temperature in electron-volts, I_a is the anode current, and I_d is the discharge current. The following equation represents the radiative power loss from the plasma:

$$P_r = n_o n_e \langle \sigma * v_e \rangle V_{pr}, \quad (5)$$

where n_o is the neutral density, $<\sigma^* v_e>$ is the excitation rate coefficient that includes the excitation cross-section and the electron velocity, and V_{pr} is the volume of the high temperature plasma region. For the power to produce ions, we have the following equation:

$$P_{ions} = (I_b + I_{iw})U^+, \quad (6)$$

where I_{iw} is the ionic current to the wall, and U^+ ionization potential. The following equation was used for the pre-sheath ion energy [6]:

$$\varepsilon = 0.58\frac{kT_e}{e}. \quad (7)$$

The equations effectively used to calculate the dissipated thermal powers in the walls and in the anode (parts in contact with the plasma) were equations (3), (4) and (7). First, the total dissipated thermal power in the walls and the dissipated thermal power in the anode were calculated for the PHALL II-C, both for the discharge power of 195.00W and for 470.53W. The values of the parameters used in the equations can be found in Table 4 (in the case of the values measured experimentally) and in Table 5, while the values of the calculated powers can be found in Table 6. The values obtained experimentally are internal experimental data and were measured using a Langmuir probe, whose tip was placed in the plasma plume 20cm from the PHALL II-C thruster.

From Table 4, V_p is the plasma potential, V_f is the floating potential, T_{eV} is the electron temperature in electron-volts, and n_e is the electron density.

Table 4: Average Data for PHALL II-C Performance

Parameters	Discharge Power 195.00W (Anode: 78.00V, 2.50A)	Discharge Power 470.53W (Anode: 105.50V, 4.46A)
$V_p\,(V)$	77.00	104.00
$V_f\,(V)$	8.00	10.00
$T_{eV}\,(eV)$	4.28	5.61
$n_e\,(m^{-3})$	2.06×10^{16}	2.13×10^{16}

Table 5: Data for PHALL II-C

Parameters	Discharge Power 195.00W (Anode: 78.00V, 2.50A)	Discharge Power 470.53W (Anode: 105.50V, 4.46A)
$T_e\,(K)$	49667.26	65101.25
$I_d\,(A)$	2.50	4.46
$e\,(C)$	1.60×10^{19}	1.60×10^{19}
$A_w\,(m2)$	3.76×10^{-3}	3.76×10^{-3}
$k\,(J/K)$	1.38×10^{-23}	1.38×10^{-23}
$m\,(kg)$	9.11×10^{-31}	9.11×10^{-31}
$M\,(kg)$	6.63×10^{-26}	6.63×10^{-26}
$\phi_S\,(V)$	-8.00	-10.00
$\varepsilon\,(V)$	2.48	3.25

Then, the ratios for walls, equation (8), and anode, equation (9), between the values of dissipated thermal power and discharge power were calculated for both the 195.00W case and the 470.53W case. After that, the average between

the two cases was calculated (Table 7). The ratio equations are shown below:

$$R_w = \frac{P_w}{P_d}, \quad (8)$$

$$R_a = \frac{P_a}{P_d}. \quad (9)$$

Where R_w is the ratio for walls, P_w is the power dissipated in the walls, P_d is the discharge power, R_a is the ratio for anode and P_a is the power dissipated in the anode.

These ratios calculated for the walls and for the anode were used to calculate, proportionally to the discharge power of the ISCT200-US, the total dissipated thermal power in the walls and the dissipated thermal power in the anode (Table 8). After that, the dissipated thermal powers in each particular wall were calculated.

Table 6: Dissipated Thermal Powers of walls and anode for PHALL II-C

Part of the PHALL II-C	For Disch. Power 195.00W	For Disch. Power 470.53W
Walls	58.89W	99.24W
Anode	21.40W	50.04W

We have that in [18] the depositions of thermal energy in the anode in the radial direction and in the internal and external walls of the discharge channel in the axial direction are practically constant, as we put in the simulation of the ISCT200-US; already the reference [19] indicates an almost constant temperature distribution in the anode and with a small variation in the internal walls (approximately from 910K to 1090K) and external (approximately from 910K to 1080K) of the discharge channel, which corroborates with the distribution of thermal energy deposition in [18]

Table 7: Ratios Between the Values of Dissipated Thermal Power and Discharge Power for PHALL II-C

Part of the PHALL II-C	For Disch. Power 195.00W	For Disch. Power 470.53W	Average
Walls	0.3020	0.2109	0.2565
Anode	0.1097	0.1064	0.1081

We need the value on each wall for the simulations. The total thermal power dissipated in the walls is the sum of the powers in each wall – see equation (8). The power division used by us was determined by analyzing [13], where the inner wall of the discharge channel heats up more than the outer wall. According to [13], the temperature of the inner wall is higher than the temperature (550K-600K) of the outer wall of the T-140 HET (Hall thruster) for a discharge power of 630W (the smallest in the study carried out in [13] and the closest to the discharge power of the ISCT200-US). Furthermore, where we have to include analysis of the relationship between the surface areas of the inner and outer walls.

Table 8: Dissipated Thermal Powers of Walls and Anode for ISCT200-US

Part of the PHALL II-C	Dissip. Thermal Power (W)
Walls	51.29
Anode	21.61

Such a relationship shows that the area of the inner wall of the PHALL II-C is approximately 60% of the area of its outer wall (the division of the area of the inner wall by the area of the outer wall is equal to 0.5958). This is an indication that the dissipated thermal power per unit area

(power density) is almost twice as high in the inner wall. Considering also that the magnetic field is stronger at the inner wall, it is expected that it will be subject to more plasma impact along magnetic field lines than the outer wall.

Because of this, a power density (power/area) ratio between the inner and outer walls of about 2:1 is expected, which is the value required to obtain a temperature difference between the inner and outer walls similar to that shown in [13].

For the center and edge walls, located in front of the thruster (Figure 3), the proportion of power density was considered equal to that of the inner wall, due to the deposition shown in PHALL II-C thruster, where the experimental data of plasma was collected. Equations (10) to (12) below were used to calculate the powers in each wall:

$$P_{wB} = P_o + P_i + P_c + P_e \tag{10}$$

$$n\frac{P_o}{A_o} = \frac{P_i}{A_i} = \frac{P_c}{A_c} = \frac{P_e}{A_e} \tag{11}$$

$$n = 2 \tag{12}$$

where P is the power in a given wall, A is the area of a given wall, the subscripts o, i, c, e refer, respectively, to the outer wall, inner wall, center wall and edge wall, with n being a factor of proportionality. The blue regions in Figure 6 indicate where the P_o, P_i, P_c e P_e powers are applied to the respective surfaces.

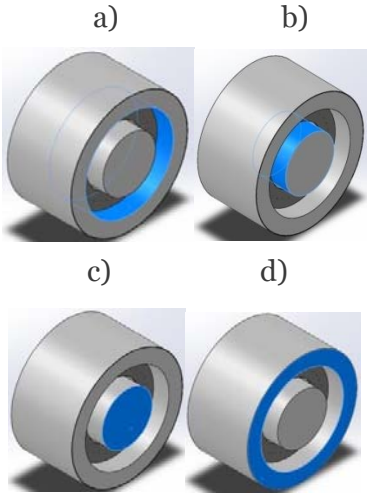

Fig. 8: Identification (blue color) of the wall surfaces considered for local power deposition in the PHALL II-C thruster: (a) outer wall, P_o, (b), inner wall, P_i, (c) central wall, P_c and (d) edge wall, P_e

For a discharge power of 200 W, the dissipated thermal powers for each part of the ISCT200-US are found in Table 9.

Table 9: Dissipated thermal powers for the ISCT200-US thruster

Part of the ISCT200-US	Power (W)
Anode	21.61
Inner Wall	9.25
Outer Wall	8.17
Central Wall	4.49
Edge Wall	29.38

3.2 The Thermal Model

The thermal model was determined from the theoretical manual [20] of the commercial software used (SolidWorks 2017, from the manufacturer Dassault Systemes). For simulation calculations, the geometry of the solid that forms

the thruster is divided into smaller parts - called finite elements (Figure 9); In this way, the structure of the solid becomes a discrete system with a set of discrete equations for the thermal model:

$$[C_T]\left[\frac{\partial T}{\partial t}\right] + [K]\{T\} = \{R\}. \quad (13)$$

Fig. 9: Mechanical Drawing of the ISCT200-US Thruster With the Subdivision of the Solid Into Finite Elements

In this case, T is the temperature at the element and is given by:

$$T = [D]\{T_n\}, \quad (14)$$

where *[D]* is a vector of shape or interpolation functions (depends on the position of the element), *{Tn}* Is a column vector of nodal temperatures and possible temperature derivatives. $[C_T]$ is calculated by equation (15).

$$[C_T] = \iiint_{\Delta V} \rho\, c [D]^T [D] dV, \quad (15)$$

where ΔV is the volume of the element, ρ is the mass density, and c is the specific heat. The other parameters are calculated according to equations (16) to (18)

$$[K] = [K_T], \quad (16)$$

with

$$[K_T] = \iiint_{\Delta V} [B]^T [k][B] dV, \quad (17)$$

$$[B] = \begin{Bmatrix} \frac{\partial D}{\partial x} \\ \frac{\partial D}{\partial y} \\ \frac{\partial D}{\partial z} \end{Bmatrix}. \quad (18)$$

Futhermore,

$$\{R\} = \{R_Q\} - \{R_q\}, \quad (19)$$

where *[k]* is the thermal conductivity and being

$$\{R_Q\} = \iiint_{\Delta V} Q\, [D]^T dV, \quad (20)$$

where Q is the internally generated heat flux, and the last parameter, $\{R_q\}$ is calculated as shown in equation (21).

$$\{R_q\} = \iint_{\Delta Sq} q\, [D]^T dS, \quad (21)$$

where ΔS_q is the boundary portion of the element and q is the boundary heat flux.

VI. RESULTS AND DISCUSSION

Starting with a simulation diagram of the ISCT200-US (Figure 10), the results obtained in the present work are presented below.

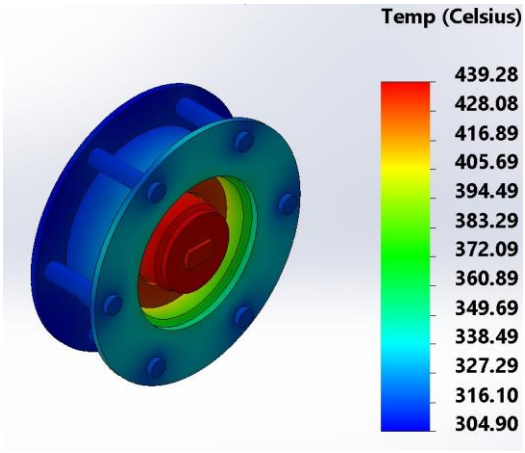

Fig. 10: ISCT200-US thruster simulation diagram

Regarding the three ISCT200-US regions considered in the experiment, the average temperatures achieved in the simulation and the experimental average temperatures presented in reference [10] are available in Table 10.

Table 10: Average Simulation Temperatures and Average Experimental Temperatures for the ISCT200-US Thruster

ISCT200-US	Anode (°C)	Inner Wall (°C)	Outer Wall (°C)
Experiment	440.00	420.00	413.00
Simulation	429.38	436.29	396.32
Difference	10.62	16.29	16.68
Percentage Difference	2.41%	3.88%	4.04%

The results obtained in the three regions considered (anode, internal wall and external wall) were very faithful to those presented by the experiments in reference [10], as a temperature difference (Table 10) between the experimental and simulated values was quite low, with an error (in percentage) having a variation between 2.41% and 4.04%.

It is estimated that the temperature difference between experimental and simulated data would be even smaller if the thermal contact resistances and all materials properly used in the ISCT200-US thruster were included in the simulation.

It is believed that the theoretical reliability of the equations for dissipated thermal power is reinforced due to the fact that they are used in the simulation to confirm the experimental data.

Due to the good results found, with the help of the equations, it appears that the simulation software is reliable.

Therefore, as the results indicate, future simulations of Hall thruster models with permanent magnets carried out using a tool based on finite elements will also be reliable for validation before obtaining experimental data.

These results also corroborate the developments in reference [11], in addition to providing greater precision. In reference [11], similar work was carried out with the BPT-4000 literature thruster.

V. CONCLUSIONS

A thermal numerical simulation of a Hall thruster found in the literature, called ISCT200-US, was carried out, in which the experimental data

provided by the literature were compared with simulation results in order to verify the reliability of the simulation tool and the corroboration of the results with a work carried out with Hall BPT-4000 thruster. The difference between the experiment and simulation temperatures was small. The percentage of difference varied between 2.41% and 4.04%, which indicates that the simulation software and the approximations used present good reliability when applied to Hall thrusters, in addition to confirming the results found in [11] for the BPT-4000.

ACKNOWLEDGMENTS

Marconi C. Porto thanks CAPES for the support in the form of a Master's Degree Scholarship.

REFERENCES

1. J. L. Ferreira, A. A. Martins, R. A. Miranda, M. C. F. Porto, H. O. Coelho, Hall plasma thruster devlopment for micro and nano satellites, J. Phys.: Conf. Ser. 1365 012026 (2019).
2. J. L. Ferreira, A. A. Martins, R. A. Miranda, A. Schelling, L. S. Alves, E. G. Costa, H. O. Coelho, A. C. Branco, F. N. O. Lopes, Permanent magnet Hall thruster development and applications on future brazilian space missions, J. Phys.: Conf. Ser. 641 012016 (2015).
3. S. Reilly, M. Sekerak, R. Hofer, Transient Thermal Analisys of the 12.5 kW Hermes Hall Thruster, 52nd AIAA/SAE/ASEE Joint Prop. Conf. AIAA 2016-5024 (2016).
4. N. Turan, U. Kokal, M. Celik, H. Kurt, Experimental Study of the Effects of the Cathode Position and the Electrical Circuit Configuration on the operation Hall Thruster Bustlab Hollow Cathode, 52nd AIAA/SAE/ASEE Joint Prop. Conf. AIAA 2016-4834 (2016).
5. R. W. Conversano, Low-Power Magneticaly Shielded Hall Thrusters, PhD Thesis, University of California. (2015).
6. D. M. Goebel, I. Katz, Fundamentals of Electrical Propulsion, John Wiley. (2008).
7. R. W. Conversano, R. B. Lobbia, K. C. Tilley, D. M. Goebel, S. W. Reilley, I. G. Mikellides, R. R. Hofer, Development and Initial Performance Testing of a LowPower Magnetically Shielded Hall Thruster with an Internally-Mounted Hollow Cathode, 35th Int. Elec. Prop. Conf. IEPC-2017-64 (2017).
8. A. A. Martins, M. C. F. Porto, H. O. Coelho, J. L. Ferreira, I. S. Ferreira, Preliminary experimental results of the PHALL II-C with improved magnetic circuit design and hollow cathode, J. Phys.: Conf. Ser. 1365 012025 (2019).
9. R. A. Miranda, A. A. Martins, J. L. Ferreira, Particle-in-cell numerical simulations of a cylindrical Hall thruster with permanent magnets, J. Phys.: Conf. Ser. 911 02021 (2017).
10. L. Grimaud, S. Mazouffre, Ion behavior in low-power magnetically shielded and unshielded Hall thrusters, Plasma Sources Sci. Technol. 26 (2017) 055020.
11. M. C. Porto, A. A. Martins, J. L. Ferreira, C. H. Llanos, Comparative analysis of simulation and experiment for the Hall-type thruster BPT-4000, Results in Engineering, 17 (2023) 101006.
12. R. W. Conversano, D. M. Goebel, R. R. Hofer, T. S. Matlock, R. E. Wirz Magnetically Shielded Miniature Hall Thruster: Development and Initial Testing, 33rd Int. Elec. Prop. Conf. IEPC-2013-201 (2013).
13. R. A. Martinez, H. Dao, M. L. R. Walker, Power deposition into the discharge channel of a hall effect thruster, Journal of Propulsion and Power. (2014) Vol. 30, No. 1, 209220, DOI: 10.2514/1.B34897.
14. L. Grimaud, S. Mazouffre, Performance comparision between standard and magnetically shielded 200 W Hall thrusters with BN-SiO_2 and graphite channel walls, 35th Int. Elec. Prop. Conf. IEPC-2017-127 (2017).
15. L. Grimaud, S. Mazouffre, Conducting wall Hall thrusters in magnetic shielding and standard configurations, Journal of Applied Physics 122, 033305 (2017).
16. S. Mazouffre, L. Grimaud, S. Tsikata, K. Matyash, R Scheinder, Investigation of rotating spoke instabilities in a wall-less Hall thruster. Part I: Experiments, 35th Int. Elec. Prop. Conf. IEPC-2017-248 (2017).

17. A. Spethmann, T. Trottenberg, H. Kersten, F. G. Hey, L. Grimaud, S. Mazouffre, Application of force measuring probes for the investigation of sputtering and as diagnostic for HEMP and Hall thrusters, 35th Int. Elec. Prop. Conf. IEPC-2017-245 (2017).
18. L. Yan, P. Wang, H. Ouyang, X Kang. Thermal analisys of the Hall Thruster in vacuum, Vacuum. (2014) Vol. 108, 40-55.
19. R. A. Martinez, M. R. L. Walker, Propellant thermal management effect on neutral residence time in low-voltage Hall thrusters, Journal of Propulsion and Power. (2013) Vol. 29, No. 3 528-539, DOI: 10.2514/1.B34702.
20. Dassault Systemes, Theoretical Manual for SolidWorks. (2017).